Strong particle dispersion by weakly dissipative random internal waves

By O L I V E R   B Ü H L E R[1]†,
N I C O L A S   G R I S O U A R D[1,2] AND M I R A N D A   H O L M E S–
C E R F O N[1]

[1]Center for Atmosphere Ocean Science at the Courant Institute of Mathematical Sciences
New York University, New York, NY 10012, USA

[2]Department of Environmental Earth System Science, Stanford University, CA 94305, USA

Simple stochastic models and direct nonlinear numerical simulations of three-dimensional internal waves are combined in order to understand the strong horizontal particle dispersion at second order in wave amplitude that arises when small-amplitude internal waves are exposed to weak dissipation. This is contrasted with the well-known results for perfectly inviscid internal waves, in which such dispersion arises only at fourth order in wave amplitude.

---

1. Introduction

We report on a somewhat surprising numerical result and on its tentative theoretical explanation in connection with our previous studies of particle dispersion by random waves in Bühler & Holmes-Cerfon (2009) and Holmes-Cerfon *et al.* (2011) (hereafter HBF). These studies addressed the fundamental question as to how non-breaking small-amplitude gravity waves can contribute to the irreversible quasi-horizontal spreading of particles along stratification surfaces at very small scales, all with an eye towards applications in oceanography. In common with previous studies of similar questions (e.g., Herterich & Hasselmann (1982), Sanderson & Okubo (1988), Weichman & Glazman (2000), Balk *et al.* (2004); Balk (2006)), we modelled the linear wave field as a stationary random process with a power spectrum that is strictly zero at zero frequency, which implies that the linear velocity field cannot by itself give rise to any diffusion in the sense of Taylor (1921) (cf. § 2 below). The physical motivation for this assumption was that the frequency of inertia–gravity waves is bounded from below by the Coriolis parameter f, which provides a natural non-zero frequency cut-off everywhere away from the equator.

This implied that particle diffusion could arise only via advection by the wave-induced Lagrangian-mean flow at second order in wave amplitude. Specifically, if in terms of the non-dimensional wave amplitude $a \ll 1$ the usual wave energy E_0 and the wave-induced Lagrangian-mean flow are $O(a^2)$, then the leading-order diffusivity D, which is quadratic in the advecting velocity, satisfies $D = O(a^4)$, i.e., $D \propto E_0^2$. Our implicit presumption was that this result, which was derived assuming unforced and inviscid random waves, would continue to hold approximately for waves that are maintained in a prescribed stationary state by the combination of weak forcing and damping, provided only that the damping rate α, say, is reasonably small compared to the frequencies of the waves.

† Author to whom correspondence should be addressed.

However, recent direct nonlinear numerical simulations of internal waves in the three-dimensional rotating Boussinesq system (detailed below in § 4) instead robustly produced values for D that were in fact proportional to E_0, and not to E_0^2 as predicted by theory. This held even for quite weak wave damping and forcing (e.g., the damping rate is only 2% of the wave frequency in the typical case displayed in figure 3 below). Notably, for small wave amplitude $a \ll 1$ the numerically observed $O(a^2)$ particle diffusion was therefore much *stronger* than the $O(a^4)$ diffusivity predicted by the inviscid theory.

Our subsequent attempt at understanding this surprising result is based on the sequence of simple stochastic models for forced–dissipative waves enumerated in § 3. These simple models allow detailed investigations into the interplay between damping and diffusion and they show clearly that adding damping is a singular perturbation to the previous inviscid theory: any fixed nonzero amount of damping leads to a diffusivity D that is proportional to the wave energy $E_0 = O(a^2)$ rather than $O(a^4)$ in the limit of small wave amplitude $a \ll 1$. In hindsight this result is perhaps less surprising, because the lack of particle diffusion at $O(a^2)$ in the inviscid theory relied crucially on the exquisite reversibility of linear particle displacements, which is lost if any nonzero amount of damping is introduced. This is the physical basis for the singular perturbation that we observed, i.e., the dramatic change from weak, $O(a^4)$ particle diffusion to strong, $O(a^2)$ particle diffusion induced by the introduction of weak dissipation.

The paper is organized as follows. The kinematics of Taylor diffusivity are summarized in § 2 and the simple stochastic models are discussed in § 3. The numerical simulations are detailed and compared to predictions from the simple models in § 4, which includes an explicit scaling law for D in § 4.3. Concluding comments are offered in § 5.

2. Kinematics of Taylor diffusivity

The diffusivity of Taylor (1921) as a measure of particle dispersion is the simplest quantity that is relevant to understanding the spreading of passive tracers within a fluid body. The basic theory applies to the time-evolution of a Cartesian particle coordinate $X(t)$ defined as

$$\frac{dX(t)}{dt} = u(t), \quad X(0) = 0, \quad \Rightarrow \quad X(t) = \int_0^t u(s)\, ds. \tag{2.1}$$

Here $u(t)$ is the corresponding Cartesian component of the velocity field, which is clearly the Lagrangian velocity field following the fluid particle. We will assume throughout that $u(t)$ is a stationary zero-mean random function with covariance function

$$C(s) = C(-s) = \mathbb{E}[u(t)u(t+s)] \quad \text{such that} \quad \frac{1}{2}\frac{d}{dt}\mathbb{E}[X^2] = \int_0^t C(s)\, ds. \tag{2.2}$$

Here $\mathbb{E}$ denotes probabilistic expectation. Assuming this integral converges as $t \to \infty$, this yields the definition of the diffusivity D, i.e,

$$D = \int_0^\infty C(s)\, ds = \frac{1}{2}\hat{C}(0) \quad \text{such that} \quad \mathbb{E}[X^2] \sim 2Dt \quad \text{for large } t. \tag{2.3}$$

The second form for D uses the power spectrum $\hat{C}(\omega)$ defined via the Fourier transform

$$\hat{C}(\omega) = \int_{-\infty}^{+\infty} e^{-i\omega s} C(s)\, ds \quad \text{and} \quad C(s) = \frac{1}{2\pi}\int_{-\infty}^{+\infty} e^{+i\omega s} \hat{C}(\omega)\, d\omega. \tag{2.4}$$

Finally, if we define the Lagrangian auto-correlation time scale as

$$\tau = \int_0^\infty \frac{C(s)}{C(0)}\,ds = \frac{1}{2}\frac{\hat{C}(0)}{C(0)} = \frac{D}{\mathbb{E}[u^2]} \quad \text{then} \quad D = \mathbb{E}[u^2]\,\tau. \tag{2.5}$$

At fixed $\mathbb{E}[u^2]$ the diffusivity D is simply proportional to τ.

3. Simple stochastic models for forced–dissipative velocity fields

We consider three simple, exactly solvable linear stochastic differential equation (SDE) models for the forced–dissipative evolution of a wavelike Lagrangian velocity field u. Common to these models is that there is a one-parameter family of possible combinations of forcing and dissipation parameters that maintain the same variance $\mathbb{E}[u^2]$, but change the time scale τ and therefore the diffusivity D. This is the key step in order to understand the direct numerical simulations of forced–dissipative waves that follow in § 4. The three models are gently increasing in complexity and relevance, and the third model, which encompasses the other two in suitable limits, provides the best theoretical guidance for understanding the full internal wave problem.

3.1. *Ornstein–Uhlenbeck process*

The Ornstein–Uhlenbeck (OU) process for $u(t)$ is defined by the SDE

$$\frac{du}{dt} + \alpha u = \beta\xi \quad \text{with} \quad \mathbb{E}[\xi] = 0 \quad \text{and} \quad \mathbb{E}[\xi(t_1)\xi(t_2)] = \delta(t_1 - t_2). \tag{3.1}$$

Here the constant parameters $\alpha > 0$ and β quantify the damping rate and forcing strength, respectively. Strictly speaking, the white noise forcing $\xi(t)$ is not a function but a distribution, and it merely serves as a convenient shorthand for the increment of the Wiener process $dW = \xi\,dt$ that necessarily appears in the general theory of SDEs (e.g. Gardiner 1997). This is sufficient for the simple additive noise examples we are studying here, but would have to be reconsidered in the case of multiplicative noise, where β depends on u. The OU process has a stationary distribution with (see §6.1)

$$\hat{C}(\omega) = \frac{\beta^2}{\omega^2 + \alpha^2} \quad \text{and} \quad C(s) = \frac{\beta^2}{2\alpha}e^{-\alpha|s|}. \tag{3.2}$$

The variance is $\mathbb{E}[u^2] = C(0) = \beta^2/2\alpha$ and hence for the OU process constant variance of u implies the one-parameter family $\beta^2 \propto \alpha$. It then follows from (2.3) and (2.5) that

$$\text{Ornstein–Uhlenbeck:} \quad D = \frac{\beta^2}{2\alpha^2} = \left(\frac{\beta^2}{2\alpha}\right)\frac{1}{\alpha} \quad \Rightarrow \quad \tau = \frac{1}{\alpha}. \tag{3.3}$$

This illustrates the well-known fact that the OU auto-correlation time scale τ is equal to the damping time scale $1/\alpha$. In particular, as the damping rate goes to zero the diffusivity at fixed variance goes to infinity.

As a model for forced–dissipative linear waves the OU process neatly illustrates the general point that D is not fixed, but depends on the modelling choice for the damping rate α. However, the absence of any intrinsic wave dynamics in the evolution equation for $u(t)$ rather limits the direct utility of the OU process for the problem at hand. The two following models improve on this point.

3.2. *Linear harmonic oscillator*

The linear harmonic oscillator (LHO) is defined by the second-order equation

$$\frac{d^2u}{dt^2} + \alpha\frac{du}{dt} + \omega_0^2 u = \beta\omega_0\xi \tag{3.4}$$

where the new parameter $\omega_0 > 0$ is the natural frequency of the undamped oscillator and β measures the white noise forcing strength as before (the factor ω_0 has been inserted to keep the units of β the same as in (3.1)). Damped oscillatory motion occurs for values of α below the threshold $\alpha = 2\omega_0$. The case of weak damping, in which $\alpha \ll \omega_0$, is perhaps the most relevant in practice, but we can actually calculate all our results here without restriction on the size of α. In particular, we obtain (see §6.1)

$$\hat{C}(\omega) = \frac{\beta^2 \omega_0^2}{(\omega^2 - \omega_0^2)^2 + \alpha^2 \omega^2} \quad \text{and} \quad D = \frac{\beta^2}{2\omega_0^2}. \tag{3.5}$$

Remarkably, the diffusivity is independent of α in this expression. However, what is relevant for us here is the diffusivity at fixed variance of u, and for this we need the covariance function, which for $\alpha < 2\omega_0$ is

$$C(s) = \frac{\beta^2}{2\alpha} e^{-\frac{\alpha|s|}{2}} \left\{ \cos(\gamma s) + \frac{\alpha}{2\gamma} \sin(\gamma |s|) \right\} \quad \text{with} \quad \gamma = \sqrt{\left| \omega_0^2 - \frac{\alpha^2}{4} \right|}. \tag{3.6}$$

In the complementary case $\alpha > 2\omega_0$ the functions $(\cos, \sin)$ are replaced by $(\cosh, \sinh)$, respectively. Either way the variance is again $\mathbb{E}[u^2] = C(0) = \beta^2/2\alpha$ and we obtain

$$\text{Linear harmonic oscillator:} \quad D = \frac{\beta^2}{2\omega_0^2} = \left(\frac{\beta^2}{2\alpha} \right) \frac{\alpha}{\omega_0^2} \quad \Rightarrow \quad \tau = \frac{\alpha}{\omega_0^2}. \tag{3.7}$$

This remarkable formula shows that at fixed ω_0 and $\mathbb{E}[u^2]$ the diffusivity is proportional to the damping rate α and accordingly goes to zero as $\alpha \to 0$. This limit is consistent with the earlier argument that a freely evolving linear wave with nonzero frequency (i.e., $\omega_0 > 0$) has $D = 0$. However, we also see that any amount of damping, no matter how small, breaks this condition and delivers a nonzero D according to (3.7).

Now, as a model for a linear wave velocity u the LHO improves on the OU process by introducing a natural wave frequency ω_0. Still, in a fluid-dynamical model one would add random forcing in the equation for du/dt, whereas in the LHO equation the forcing acts on d^2u/dt^2 instead. This leads us to the third model.

3.3. *Inertial oscillations*

The third model is based on the inertial oscillations of a horizontally homogeneous single fluid layer relative to a state of rest in a rotating frame of reference with Coriolis parameter f, say. The horizontal velocity vector $\boldsymbol{u} = (u, v)$ and the governing SDEs are

$$\frac{du}{dt} + \alpha u - fv = \beta \xi_1 \quad \text{and} \quad \frac{dv}{dt} + \alpha v + fu = \beta \xi_2. \tag{3.8}$$

Here $\xi_1(t)$ and $\xi_2(t)$ are independent versions of white noise. In the stationary regime u and v are identically distributed and for their common power spectrum and autocorrelation function we obtain (see §6.1)

$$\hat{C}(\omega) = \frac{1}{2} \left(\frac{\beta^2}{(\omega + f)^2 + \alpha^2} + \frac{\beta^2}{(\omega - f)^2 + \alpha^2} \right) \quad \text{and} \quad C(s) = \frac{\beta^2}{2\alpha} \cos(fs) e^{-\alpha|s|}. \tag{3.9}$$

Comparing (3.9) with (3.2) it is clear that this is the natural generalization of the OU process to the case of a natural wave frequency f. Once more the variance of u is $\beta^2/2\alpha$ and the diffusivity is

$$\text{Inertial oscillations:} \quad D = \frac{1}{2} \frac{\beta^2}{f^2 + \alpha^2} = \left(\frac{\beta^2}{2\alpha} \right) \frac{\alpha}{f^2 + \alpha^2} \quad \Rightarrow \quad \tau = \frac{\alpha}{f^2 + \alpha^2}. \tag{3.10}$$

The time scale of this process interpolates between the former two: for small α it approximates the LHO with $\tau \propto \alpha$ whilst for large α it approximates the OU process with $\tau \propto 1/\alpha$. As will be shown below, this is essentially what we observe for the Taylor diffusivity in direct numerical simulations of wave-induced particle dispersion due to forced–dissipative internal gravity waves.

4. Direct numerical simulations

We describe direct numerical simulations of small-amplitude internal waves using a fully nonlinear three-dimensional numerical model for the rotating Boussinesq system with linear damping and white noise wave forcing in time.

4.1. *Numerical set-up*

We use a modification of the pseudo-spectral model of Winters *et al.* (2004), which solves

$$\boldsymbol{u}_t + (\boldsymbol{u} \cdot \boldsymbol{\nabla})\boldsymbol{u} + f\hat{\boldsymbol{z}} \times \boldsymbol{u} + \boldsymbol{\nabla}P - b\hat{\boldsymbol{z}} = +\mathcal{D}_6 \boldsymbol{u} - \alpha_q \boldsymbol{u}_q + \boldsymbol{F}, \tag{4.1a}$$

$$b_t + (\boldsymbol{u} \cdot \boldsymbol{\nabla})b + N^2 w = +\mathcal{D}_6 b - \alpha_q b_q, \quad \text{and} \quad \boldsymbol{\nabla} \cdot \boldsymbol{u} = 0 \tag{4.1b}$$

Here $\boldsymbol{u} = (u, v, w)$ is the velocity vector, $f = 10^{-4}$ s^{-1} is the Coriolis parameter, $\hat{\boldsymbol{z}}$ is the vertical unit vector, P is the scaled pressure fluctuation, b is the buoyancy, and $N = 10^{-3}$ s^{-1} is the constant buoyancy frequency. The dissipation operator $\mathcal{D}_6$ is

$$\mathcal{D}_6 = - \left(\nu_{6H} (\partial_x^2 + \partial_y^2)^3 + \nu_{6z} \partial_z^6 \right), \tag{4.2}$$

where ν_{6H} and ν_{6z} are horizontal and vertical dissipation coefficients. The additional damping related to α_q is discussed below (4.6). Our numerical domain is a triply periodic rectangular box with horizontally square cross-section of side length $L = 1$ km and vertical height $H = \delta L = 100$ m, so the aspect ratio $\delta = f/N = 1/10$. The numerical grid is flattened in the vertical and the domain is discretized with $n = 96$ points in all three directions. We choose $\nu_{6z} = \delta^6 \nu_{6H}$.

All fields X are expanded into discrete Fourier series of the form

$$X(x, y, z, t) = \sum_{k,l,m} \widetilde{X}_{klm}(t) \exp \mathrm{i} \, (kx + ly + mz), \tag{4.3}$$

where $(k, l, \delta m)$ can take values from the discrete sets $\{-n/2 + 1, \dots, n/2\} \times 2\pi/L$. The reality condition $\widetilde{X}^*_{-(klm)} = \widetilde{X}_{klm}$ is enforced numerically by evolving the fields for $k > 0$ only and then extending the results to $k < 0$ by complex conjugation.

The white noise in time wave forcing $\boldsymbol{F}$ is designed to have no effect on the linear potential vorticity (PV) of the system, which is $q = \hat{\boldsymbol{z}} \cdot (\boldsymbol{\nabla} \times \boldsymbol{u}) + fb_z/N^2$. Otherwise the forcing would produce an unwanted balanced, PV-controlled flow at the same order as the waves, which would dominate the particle advection. This requires that $\hat{\boldsymbol{z}} \cdot (\boldsymbol{\nabla} \times \boldsymbol{F}) = 0$, and we also find it convenient to enforce $\boldsymbol{\nabla} \cdot \boldsymbol{F} = 0$ because any divergent part of $\boldsymbol{F}$ is absorbed by the pressure gradient. In spectral space this is achieved by

$$\widetilde{\boldsymbol{F}}_{klm}(t) = \frac{1}{k_H K} \begin{bmatrix} -km \\ -lm \\ k_H^2 \end{bmatrix} \xi(t) \quad \text{and} \quad \widetilde{\boldsymbol{F}}^*_{-(klm)}(t) = \widetilde{\boldsymbol{F}}_{klm}(t), \tag{4.4}$$

where $K = \sqrt{k_H^2 + m^2}$. Here $\xi = \xi_R + i\xi_I$ is a complex normal random variable (independent from time step to time step) with independent real and imaginary parts ξ_R and ξ_I such that at each numerical time step with step size Δt

$$\mathbb{E}\left[\xi_{R,I}\right] = 0, \quad \mathbb{E}\left[\xi_R \xi_I\right] = 0, \quad \text{and} \quad \mathbb{E}\left[\xi_{R,I}^2\right] = 2\alpha_{k_H m} E_{klm}/\Delta t. \tag{4.5}$$

Here $\alpha_{k_Hm} = \nu_{6H}k_H^6 + \nu_{6z}m^6$, $\Delta t = 100$ s the numerical time step and E_{klm} is a spectral energy density that is related to the expected energy by

$$E_0 = \frac{1}{2}\mathbb{E}\left[u^2 + v^2 + w^2 + \frac{b^2}{N^2}\right] = \sum_{k,l,m} E_{klm}. \tag{4.6}$$

For time stepping a third-order Adams-Bashforth (AB3) scheme is used for all terms except the random force, which is instead advanced using forward Euler. To minimize aliasing whilst maintaining numerical accuracy, $1/9^{\text{th}}$ of the wavenumbers are truncated following Patterson & Orszag (1971).

There is one important caveat that we need to mention. Although $\boldsymbol{F}$ as defined does not project onto the *linear* PV, in the presence of internal waves it does project on the exact *nonlinear* PV defined by $Q = \boldsymbol{\nabla}(N^2z + b) \cdot (\boldsymbol{\nabla} \times \boldsymbol{u} + f\hat{\boldsymbol{z}})$ via the $O(a^2)$ forcing term $\boldsymbol{\nabla}b \cdot (\boldsymbol{\nabla} \times \boldsymbol{F})$, which will produce an unwanted balanced flow at $O(a^2)$. Although this is much smaller than the $O(a)$ waves, this nearly steady balanced flow can still lead to significant particle advection and hence we have found it necessary to continuously damp the balanced flow. To this end we diagnose at each time step the linear balanced flow $(\boldsymbol{u}_q, b_q)$ from the instantaneous q via a quasi-geostrophic stream function ψ, i.e.,

$$\psi_{xx} + \psi_{yy} + \frac{f^2}{N^2}\psi_{zz} = q \quad \text{and} \quad u_q = -\psi_y, \quad v_q = \psi_x, \quad w_q = 0, \quad b_q = f\psi_z. \tag{4.7}$$

This linear balanced flow is then damped with decay rate $\alpha_q = 1/250$ s^{-1}.

4.2. *Results for particle dispersion and diffusivity D*

All numerical experiments are executed using the same functional form of the wave energy spectrum localized at a central frequency ω_0 and a scaled wavenumber K_{s0} via

$$E_{klm} = (E_0/n_F) \times 1_{-\Delta\omega/2 \leq \omega - \omega_0 \leq +\Delta\omega/2} \times 1_{-\Delta K_s/2 \leq K_s - K_{s0} \leq +\Delta K_s/2}. \tag{4.8}$$

Here n_F is the number of modes for which $E_{klm} \neq 0$, the indicator function 1_X is unity if X is true and zero otherwise, and

$$K_s(k_H, m) = \frac{L\sqrt{k_H^2 + \delta^2m^2}}{\pi n} \quad \text{and} \quad \omega(k_H, m) = \frac{\sqrt{k_H^2N^2 + m^2f^2}}{K} \tag{4.9}$$

are the scaled total wavenumber and the positive inertia–gravity wave frequency. We use $\omega_0/f = 2.06$, $\Delta\omega/f = 2.01$, $K_{s0} = 0.56$ and $\Delta K_s = 0.08$. Hence the central wave has horizontal and vertical wavelengths of about 43 and 8 metres, respectively, and its frequency is near-inertial, which makes the simple model § 3.3 relevant with ω_0 replacing f. Figure 1 shows snapshots of the wave field in both physical and spectral space, where the signature of the forcing in spectral space is clearly seen. The damping rate α_{k_Hm} does not vary much over the range of excited wavenumbers in (4.8) and we will simply denote its average over these wavenumbers by α_0.

We seed the fluid with 64 Lagrangian particles in a regular $4 \times 4 \times 4$ pattern (see figure 2). To maximize the distance between particles, a rudimentary staggering of the initial horizontal positions across the vertical direction is implemented. Finally, contrary to what is described in Winters *et al.* (2004), the velocity at each particle position is interpolated from the Eulerian velocities at the neighboring grid points, without communication between processors in parallel configurations, and an AB3 scheme is used to advect the particles.

We assume that the particles are experiencing horizontal Taylor diffusion if

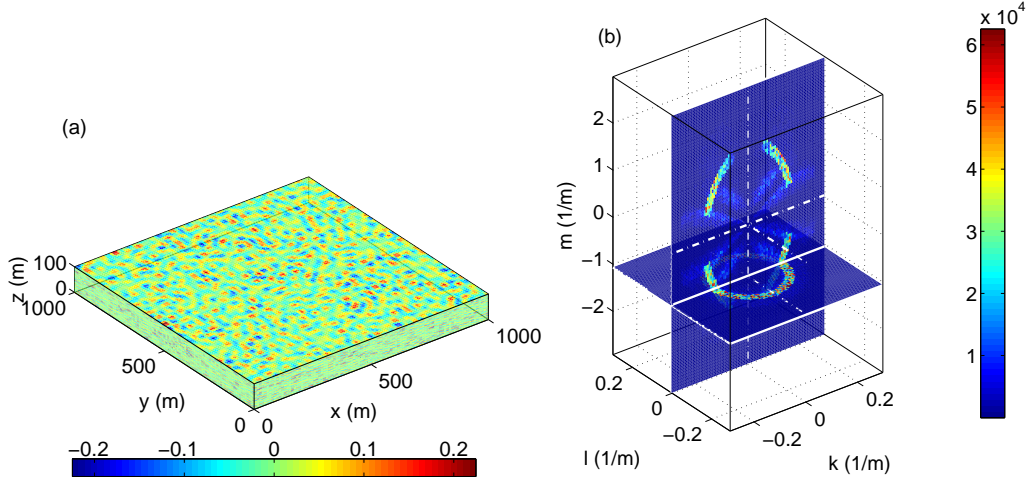$$R^2 = \mathbb{E}\left[R_i^2\right] = 4Dt, \quad \text{where} \quad R_i = \sqrt{(x_i - x_{0i})^2 + (y_i - y_{0i})^2} \tag{4.10}$$

FIGURE 1. Snapshots of the scaled horizontal divergence $(u_x + v_y)/f = -w_z/f$ for $E_0 = 2 \times 10^{-9}$ m^2 s^{-2} and $\alpha_0/\omega_0 = 2.4 \times 10^{-3}$ in (a) physical space and (b) spectral space (the absolute value of the Fourier transform is shown). The non-dimensional wave amplitude is about 10% in this example.
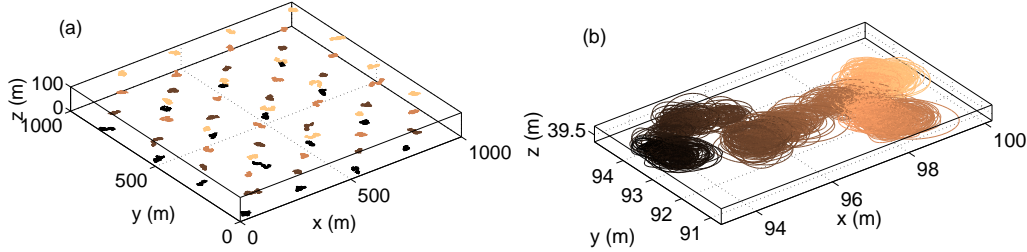

FIGURE 2. Three-dimensional view of the particle trajectories in the example from figure 1. (a) All particle trajectories, enlarged 10 times for clarity. Particles are colour-coded as a function of their initial altitude: darker means lower. (b) A single particle trajectory in real size with colour indicating time from $t = 0$ (dark) to $t = 600$ days (light). The trajectory is dominated by inertial circles superimposed on a weak random walk.

is the horizontal displacement of the ith particle. The expectation is estimated by an average over all particles and over eleven independent runs. Figure 3 shows R^2 as a function of time in two cases with weak damping, indicating that R^2 is proportional to time and also that $D \propto E_0 = O(a^2)$ instead of the inviscid prediction $D \propto E_0^2 = O(a^4)$.

4.3. *A diffusivity scaling law for very weak damping*

Letting $\alpha_0/\omega_0 \to 0$ at fixed amplitude a presumably recovers the $O(a^4)$ diffusivity of the inviscid theory. Now, for very weak damping with α_0/ω_0 comparable to $O(a^2)$ we expect this inviscid $O(a^4)$ diffusivity to be comparable to the forced–dissipative $O(a^2)$ diffusivity. In this regime we may use the theoretical prediction from § 3.2-3.3, namely that the $O(a^2)$ contribution to diffusivity is proportional to α_0. Both terms can then be taken into account in the asymptotic scaling law

$$D = \alpha_0 E_0 \, D_2 + E_0^2 \, D_4 \quad \Leftrightarrow \quad \frac{D}{E_0^2} = \left(\frac{\alpha_0}{E_0}\right) D_2 + D_4. \qquad (4.11)$$
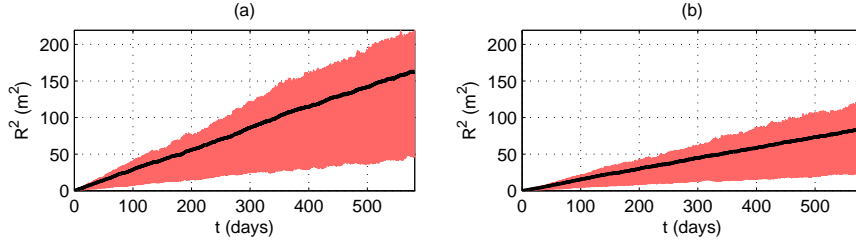
FIGURE 3. Statistics on particle displacements for $\alpha_0/\omega_0 = 2.0 \times 10^{-2}$ and (a) $E_0 = 10^{-9}$ m^2 s^{-2} and (b) $E_0 = 5 \times 10^{-10}$ m^2 s^{-2}. Shadings: area centered around the median position where 50% of the particles are found. Black lines: estimated R^2, which equals $4Dt$ under Taylor diffusion. A comparison shows very clearly that the slope $4D \propto E_0$.
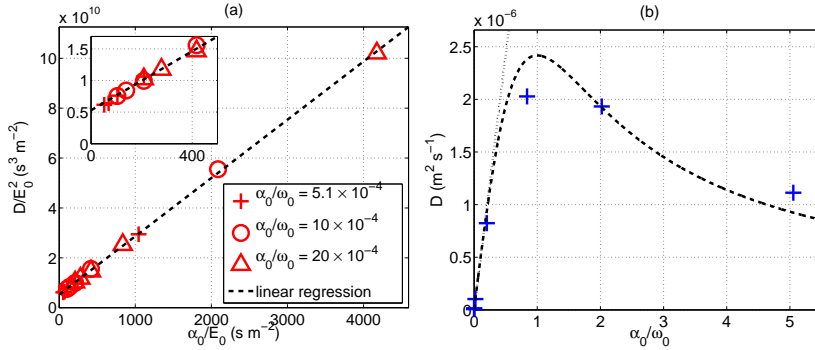

FIGURE 4. (a) D/E_0^2 as a function of α_0/E_0, with insert for deducing D_4. (b) D as a function of α_0/ω_0 with constant $E_0 = 10^{-9}$ m^2 s^{-2}. Crosses: numerical results; dotted line: tangent at origin; dashed line: $A\alpha_0/(\omega_0^2 + \alpha_0^2)$, where A is deduced from the slope at the origin.

Here the parameters D_2 and D_4 depend on the shape of the spectrum, but not on α_0 or E_0. The second form makes obvious that D/E_0^2 is just a linear function of α_0/E_0. Also, the theoretical formula (3.7) suggests $\mathbb{E}[u^2]\alpha_0/\omega_0^2 \approx \alpha_0 E_0 D_2$, which for horizontally isotropic near-inertial waves implies $D_2 \approx 1/\omega_0^2$.

To test (4.11) we conducted a series of numerical experiments varying both E_0 and α_0. Specifically, E_0 takes the values 1, 5, 10, 15 and 20×10^{-10} m^{2}s^{-2}, while $\alpha_0/\omega_0 \approx$ 5.1, 10 and 20×10^{-4}. Each of these 15 numerical experiments comprises 11–member ensembles, so that statistics for each experiment are computed on $11 \times 64 = 704$ particles. Experiments are spun up from rest and integrated for $T = 1200$ days (about 3000 wave periods) for $\alpha_0/\omega_0 \approx 5.1 \times 10^{-4}$ and 600 days otherwise. We then compute the diffusivity by averaging $R^2/4t$ over the last $1/3$ of the integration time. The results are displayed in figure 4a and show very good agreement with (4.11), yielding the numerical estimates $D_2 = 2.4 \times 10^7$ s^2 and $D_4 = 5 \times 10^9$ m^{-2} s^3.

This value for D_2 is very close to the theoretical prediction $D_2 \approx 1/\omega_0^2 = 2.5 \times 10^7$ s^2. We also cross-checked at least the order of magnitude of D_4 by applying the inviscid theory of HBF to the spectrum (4.8), which produced $D_4 = 1.8 \times 10^9$ m^{-2} s^3.

4.4. *Diffusivity for strong damping*

In a second series of experiments we explored the behaviour of D for strong damping, with α_0/ω_0 of order unity. In this regime the inviscid $O(a^4)$ contribution to D is negligible. The theoretical prediction from § 3.3 suggests that the $O(a^2)$ diffusivity should scale with $\alpha_0/(\omega_0^2 + \alpha_0^2)$, which exhibits a maximum at $\alpha_0 = \omega_0$. It is hard to check this prediction

exactly, not least because ω varies by 50% in our spectrum (4.8). Still, investigating this by a series of 600 day runs in which E_0 is kept constant at 10^{-9} m^{2}s^{-2} whilst α_0/ω_0 is varied from 5.1×10^{-4} to 5.1 led to the encouraging results shown in figure 4b.

5. Concluding comments

Our direct numerical wave simulations turned out to be compatible with the simple stochastic model based on (2.5) and (3.10) for the $O(a^2)$ horizontal diffusivity due to internal waves with frequency ω_0 and damping rate α_0:

$$D = \mathbb{E}[u^2]\, \tau = \mathbb{E}[u^2]\, \frac{\alpha_0}{\omega_0^2 + \alpha_0^2}. \tag{5.1}$$

For weak damping the relevant auto-correlation time scale is $\tau = \alpha_0/\omega_0^2$. Of course, a practical application of simple stochastic models such as (5.1) first requires an understanding of the real wave damping mechanisms, which are rarely linear and may involve wave breaking, and also a justification of the forcing model based on white noise in time. This is never an easy task in macroscopic fluid dynamics. Still, we plan to consider these ideas for the internal wave spectrum in the ocean, where estimates for the highly intermittent decay rate range from a few days to several months (e.g., Munk 1981).

There is another physical shortcoming of our simple model, namely that once we allow for realistic wave dissipation we must also allow for the concomitant generation of PV that inevitably arises at $O(a^2)$ in momentum-conserving physical systems (e.g, Bühler 2000). In our numerical model the PV was strongly damped by design, so this process was eliminated. We hope to address in the near future the interesting fundamental problem of particle dispersion due to a self-consistent ensemble of weakly dissipative waves together with their concomitant wave-induced balanced flows.

6. Appendix

6.1. *Derivation of power spectra in § 3*

By definition, the power spectrum $\hat{C}(\omega)$ of a real-valued stationary zero-mean random process $u(t)$ is the Fourier transform of $C(s) = \mathbb{E}[u(t)u(t+s)]$ with respect to the time lag s. Using (2.4) this can be written in terms of the distributional Fourier transform $\hat{u}(\omega) = \hat{u}^*(-\omega)$ as

$$\hat{C}(\omega) = \frac{1}{2\pi} \int_{-\infty}^{+\infty} e^{i(\omega-\omega')t}\, \mathbb{E}[\hat{u}(\omega)\hat{u}^*(\omega')]\, d\omega' = \frac{1}{2\pi} \int_{-\infty}^{+\infty} \mathbb{E}[\hat{u}(\omega)\hat{u}^*(\omega')]\, d\omega'. \tag{6.1}$$

The second form uses $\mathbb{E}[\hat{u}(\omega)\hat{u}^*(\omega')] = 0$ if $\omega \neq \omega'$. The distribution $\hat{u}(\omega)$ is easily expressed in terms of the distribution $\hat{\xi}(\omega) = \hat{\xi}^*(-\omega)$ by taking the Fourier transform of the governing SDE; it is this step that ensures that u follows the invariant measure of the SDE. For example, for the OU-process this yields $\hat{u} = \beta\hat{\xi}/(i\omega + \alpha)$. Evaluating (6.1) is then straightforward after noting the spectral equivalent of (3.1b):

$$\mathbb{E}[\xi(t_1)\xi(t_2)] = \delta(t_1 - t_2) \quad \Leftrightarrow \quad \mathbb{E}[\hat{\xi}(\omega)\hat{\xi}^*(\omega')] = 2\pi\, \delta(\omega - \omega'). \tag{6.2}$$

This immediately yields $\hat{C}(\omega)$ and hence the corresponding functions $C(s)$ in § 3.1-3.2.

The two-variable case in § 3.3 is best analyzed using the complex variable $z = u + iv$ such that (3.8) become the complex SDE $dz/dt + \alpha z + ifz = \beta(\xi_1 + i\xi_2)$. The equivalent of (6.1) for the transform $\hat{Q}(\omega)$ of the complex auto-correlation function

$$Q(s) = \mathbb{E}[z^*(t)z(t+s)] \quad \text{is then} \quad \hat{Q}(\omega) = \frac{1}{2\pi} \int_{-\infty}^{+\infty} \mathbb{E}[\hat{z}(\omega)\hat{z}^*(\omega')]\,d\omega'. \qquad (6.3)$$

Using $\mathbb{E}[\hat{\xi}_i(\omega)\hat{\xi}_j^*(\omega')] = 2\pi\,\delta_{ij}\delta(\omega - \omega')$ this is evaluated as

$$\hat{Q}(\omega) = \frac{2\beta^2}{(\omega + f)^2 + \alpha^2} \quad \text{and} \quad Q(s) = \frac{\beta^2}{\alpha} e^{-ifs} e^{-\alpha|s|}. \qquad (6.4)$$

Note that $Q^*(-s) = Q(s)$. From (6.3) it then follows that

$$Q(s) = \mathbb{E}[u(t)u(t+s)] + \mathbb{E}[v(t)v(t+s)] + i\left(\mathbb{E}[u(t)v(t+s)] - \mathbb{E}[u(t)v(t-s)]\right) \qquad (6.5)$$

after using stationarity for the final term. In the present case $u(t)$ and $v(t)$ are identically distributed (though not independent) and therefore

$$C(s) = \mathbb{E}[u(t)u(t+s)] = \frac{1}{2}\operatorname{Re}Q(s) = \frac{\beta^2}{2\alpha}\cos(fs)e^{-\alpha|s|}. \qquad (6.6)$$

Analogously, $\mathbb{E}[u(t)v(t+s)] = \frac{1}{2}\operatorname{Im}Q(s) = -\frac{\beta^2}{2\alpha}\sin(fs)e^{-\alpha|s|}$. Finally, (6.6) implies $\hat{C}(\omega) = (\hat{Q}(\omega) + \hat{Q}^*(-\omega))/4$, so with real $\hat{Q}(\omega)$ one can also note the shortcuts $D = \hat{Q}(0)/4$, $\mathbb{E}[u^2] = Q(0)/2$, and $\tau = \frac{1}{2}\hat{Q}(0)/Q(0)$.

REFERENCES

BALK, A.M. 2006 Wave turbulent diffusion due to the Doppler shift. *J. Stat. Mech.* **P08018**.

BALK, A.M., FALKOVICH, G. & STEPANOV, M.G. 2004 Growth of density inhomogeneities in a flow of wave turbulence. *Phys. Rev. Lett.* **92** (244504).

BÜHLER, O. 2000 On the vorticity transport due to dissipating or breaking waves in shallow-water flow. *J. Fluid Mech.* **407**, 235–263.

BÜHLER, O. & HOLMES-CERFON, M. 2009 Particle dispersion by random waves in rotating shallow water. *J. Fluid Mech.* **638**, 5–26.

GARDINER, C. W. 1997 *Handbook of Stochastic Methods.* Berlin: Springer.

HERTERICH, K. & HASSELMANN, K. 1982 The horizontal diffusion of tracers by surface waves. *Journal of Physical Oceanography* **12**, 704–712.

HOLMES-CERFON, M., BÜHLER, O. & FERRARI, R. 2011 Particle dispersion by random waves in the rotating Boussinesq system. *J. Fluid Mech.* **670**, 150–175.

MUNK, W. 1981 Internal waves and small-scale processes. *Evolution of Phys. Oceanography* pp. 264–291.

PATTERSON, G. S. & ORSZAG, S. A. 1971 Spectral Calculations of Isotropic Turbulence: Efficient Removal of Aliasing Interactions. *Physics of Fluids* **14** (11), 2538–2541.

SANDERSON, B.G. & OKUBO, A. 1988 Diffusion by internal waves. *Journal of Geophysical Research* **93**, 3570–3582.

TAYLOR, G. I. 1921 Diffusion by continuous movements. *Proc. London Math. Soc.* **20**, 196–212.

WEICHMAN, P. & GLAZMAN, R. 2000 Passive scalar transport by travelling wave fields. *Journal of Fluid Mechanics* **420**, 147–200.

WINTERS, K. B., MACKINNON, J. A. & MILLS, BREN 2004 A Spectral Model for Process Studies of Rotating, Density-Stratified Flows. *Journal of Atmospheric and Oceanic Technology* **21** (1), 69–94.